Computers and Geotechnics 161 (2023) 105512

Contents lists available at ScienceDirect

Computers and Geotechnics

journal homepage: www.elsevier.com/locate/compgeo

Modelling mesh independent failure loads of a soft strain-softening clay using a rate dependent model

Laura A. Rødvand [a,b,*], Hans Petter Jostad [a], Gustav Grimstad [b], Lars Andresen [a]

[a] Norwegian Geotechnical Institute, Oslo, Norway
[b] Norwegian University of Science and Technology, Trondheim, Norway

ARTICLE INFO

Keywords:
Localisation
Pore water flow
Destructuration
Strain rate
Finite element analysis
Regularisation

ABSTRACT

If no regularisation method is used during finite element modelling of strain-softening (brittle) materials, results become mesh dependent: manifesting as very thin shear bands whose thickness and orientation depends on the mesh discretisation. The objectives of this paper were to determine if mesh independent results were achieved, and to track the evolving width of the shear band when considering naturally occurring properties of soft clays, including a rate dependent stress-strain-strength relationship. The constitutive model included a destructuration process and strain-rate dependency, and the analyses allowed for local pore water flow. A bearing capacity problem was loaded to failure. Analyses were conducted with different mesh discretisation, loading rates and permeabilities. The results demonstrated mesh independent failure loads, and the strain-softening occurred in zones with thickness independent of mesh size. Local pore water flow delayed the initiation of strain softening and resulted in higher failure loads. The softening zones grew in thickness to over one meter, reinforcing that the finite element method is suitable for the determination of the bearing capacity of strain-softening sensitive clays. In conclusion, the rate dependent constitutive model is a promising method for regularising strain localisation in soft brittle clays under quasi-static loading conditions.

1. Introduction

Under undrained loading conditions, soft sensitive clays display brittle behaviour (strain-softening). Deformations localise into zones of intense local straining, often termed shear bands. The thickness of these shear bands has significant importance to the response of boundary value problems. In finite element analyses involving strain-softening materials, the boundary value problem may become ill-posed, resulting in shear bands where the thickness and propagation direction depends on the element size and mesh orientation. Regularisation methods may be used to achieve mesh independent results, but they typically require the introduction of an internal length scale to the model, unless some inherent property of the material at the constitutive level can provide such a regularisation. This paper investigates if the inherent rate dependency and pore water flow occurring in soft clays might provide both regularisation ability and insight into the growth of shear bands.

Rate dependency may restore the well-posedness of a boundary value problem. The regularising effect of rate dependency for single phase materials was first documented for analyses of dynamic problems (Loret and Prevost, 1991; Sluys and de Borst, 1992), where analytical analyses provided a solution for the material internal length. It is not possible to determine an internal length using analytical analysis of quasi-static problems (de Borst and Duretz, 2020); rather the ability to avoid mesh dependent results must be tested by numerical analyses with different mesh discretisation. This paper conducts numerical analyses of quasi-static problems, because the geotechnical problems of interest, such as the triggering of landslides and bearing capacity failure, are quasi-static at the moment of failure (point of global instability).

The process of strain localisation, including the initial formation and later propagation of the shear band in strain-softening sensitive clay materials is not fully understood. The formation and growth of shear bands is difficult to monitor in large-scale tests. Shear banding in small laboratory tests (Oka et al., 2005; Gylland et al., 2014; Thakur et al., 2018) indicates shear bands with evolving paths and thicknesses rather than a constant thickness throughout shearing. Therefore, a regularisation method that uses naturally occurring processes, such as strain rate dependency and pore water flow, rather than introducing a fixed artificial length scale, such as the non-local strain method (Eringen, 1981; Bazant et al., 1984), is appealing.

Strain softening may be implemented in different ways depending on the material the constitutive model should replicate. Strain softening for

* Corresponding author at: NGI, Postboks 3930 Ullevål Stadion, 0806 Oslo, Norway.
E-mail address: laura.rodvand@ngi.no (L.A. Rødvand).

https://doi.org/10.1016/j.compgeo.2023.105512
Received 28 October 2022; Received in revised form 30 April 2023; Accepted 1 May 2023
Available online 1 June 2023

Nomenclature

CSS	current stress surface
D	destructuration parameter
G	shear modulus
ICS	intrinsic compression surface
k	permeability
K	bulk modulus
M	slope of the critical state line
NCS	normal consolidation surface
p'	mean effective stress
p'_{eq}	effective equivalent mean stress
p'_{m}	effective preconsolidation pressure
p'_{mi}	effective intrinsic stress
$p'_{mi,0}$	initial effective intrinsic stress
q	deviatoric stress
r_{si}	Janbu's creep number
S_t	sensitivity
t	time
Δu	change in excess pore pressure
W_2^{int}	Second order work
x	distance along cross-section profile
β	creep ratio
χ	structure
χ_o	initial value of structure
ε	strain tensor
ε_q	deviatoric strain
$\dot{\varepsilon}_q$	deviatoric strain rate
ε_y	vertical strain
ζ	irrecoverable compressibility, $\zeta = \lambda_i^* - \kappa^*$
κ^*	modified swelling index
λ_i^*	modified compression index for remoulded soil
$\boldsymbol{\sigma'}$	effective stress tensor
τ	reference time

sand or stiff clays is achieved by reducing the friction angle and cohesion (Potts et al., 1990; di Prisco et al., 2002), however, Thakur et al. (2014) conclude that the friction angle and cohesion do not significantly reduce during undrained loading in soft, sensitive Norwegian clays. Constitutive models with a destructuration process have successfully replicated the strain-softening response of soft, sensitive clays (Yin and Karstunen, 2011; Gras et al., 2018), however the regularising ability of these types of models has not yet been investigated.

Different implementations of strain-softening or rate dependency may alter the effectiveness of rate dependency as a regularisation technique. For sand materials, di Prisco et al., (2002) and Conte et al. (2010) required a non-local strain formulation in addition to elasto-viscoplasticity to achieve mesh independent results. The shear band width is known for sands (Viggiani et al., 2001), thus the use of the non-local technique is appropriate. However, the shear band thickness is not well understood for clays, and appears to change during the failure process (Thakur et al., 2018), making the choice of a single input parameter for internal length difficult. Hence this paper will not use a non-local strain technique.

Allowing pore water flow may act as a weak regularising technique. During strain localisation in soft, sensitive Norwegian clays, contraction in the shear band results in local increases in excess pore water pressure (Thakur et al., 2018). Allowing pore water flow out of the shear band, results in higher effective stresses and shear strength within the shear band. Jostad et al. (2006) and Thakur (2011) numerically analysed the effect of local pore water drainage on strain localisation for soft clays and found that strain localisation was delayed for rate independent models. Implementation of viscoplasticity and coupled pore water flow in a clay model by Oka et al. (1995) indicated possible mesh independent results, but needed further testing with finer mesh sizes, something that is now possible with the advances in computational resources since Oka's publication.

A one-dimensional shear column case (Rødvand et al., 2022) generated mesh independent results in the strain-softening regime but was unable to provide a solution for the shear band width. A small material imperfection was required to initiate strain localisation. The shear band width was initially equal to the full height of the column, then reduced to the width of the imperfection, until a critical point was reached where the shear band thickness rapidly reduced to a width defined by the element size. Application of the same rate dependent material model in a two-dimensional boundary value problem will eliminate the need for an artificial imperfection to initiate strain localisation. The hypothesis is that allowing the shear stress distribution to vary spatially in two dimensions will permit the shear band to propagate in two-dimensional space, and thus enable measurement of the evolving shear band width.

The objective of this paper is firstly to demonstrate that for a soft strain-softening clay, the use of a soil model with strain-rate dependency and coupled pore water flow will result in mesh independent results at failure for a bearing capacity problem. Both rate dependency and pore water flow are naturally occurring processes in clay material. Secondly, the aim is to quantitively assess the width of the shear band during the loading process. The material properties used in the analyses are realistic and replicate the response of a soft, sensitive marine clay (Rødvand et al., 2022).

2. Materials and methods

This paper uses finite element modelling with a rate dependent constitutive model and coupled pore water flow to analyse a bearing capacity problem on a soft strain-softening clay. The mesh discretisation is varied to investigate the mesh dependency of the results. Loading time is varied to ensure the regularisation ability applies to a range of loading rates.

2.1. Rate dependency

Rate dependency assists in regularisation in the strain-softening regime because equal changes in stress are achieved by neighbouring elements straining at different rates. A shear band cannot localise instantaneously to one element as the strain rate increase necessary for this jump would cause a stress increase, which is incompatible with neighbouring elements that must undergo stress reduction. In Rødvand et al., (2022) it was demonstrated that gradual increases and decreases in strain rates are necessary to maintain equilibrium and simultaneously satisfy the kinematics of the displacement field. Fig. 1 presents idealised isotaches for different applied strain rates. Consider the formation of a shear band, where the largest amount of straining occurs in the centre of the shear band. The shear stresses must remain in equilibrium across the shear band. A point in the centre of the shear band (point A) may gradually accelerate and proceed to isotaches for higher strain rates. On the edge of the shear band (point B) the strain rate gradually decreases and moves through isotaches for slower strain rates. Outside the shear band, the soil may start to unload (point C), all whilst undergoing the same change in shear stress and satisfying the kinematics of the displacement field.

2.2. Constitutive model with rate dependency

The soil model used in this paper is an effective stress model based on

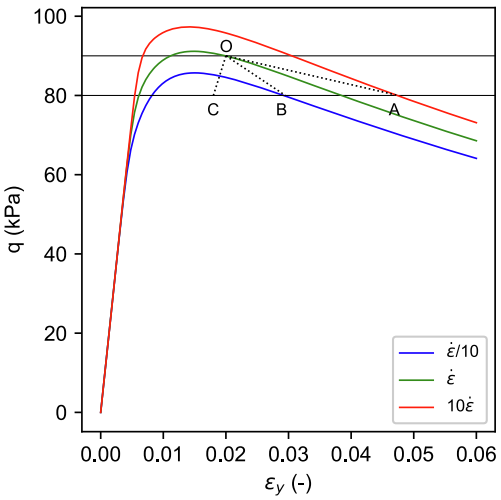

Fig. 1. Illustration of stress paths for points inside (A and B) and outside (C) the shear band. Equal changes in deviatoric stress achieved by gradual changes in strain rate. O–A = acceleration, O-B = deceleration, O-C = unloading.

the Modified Cam Clay Model: Fig. 2. A full model description is provided in Rødvand et al. (2022). The model incorporates the following features that are characteristic to soft sensitive clays:

- The strain-softening response is modelled by a destructuration process, following the method of Gens and Nova (1993), and has been shown to accurately replicate the response of real soft, sensitive clays (Yin and Karstunen, 2011). The destructuration process represents the degradation of bonding between the clay particles that occurs during plastic straining. The parameter *structure* (χ) decreases during plastic straining.
- The strain-rate dependency is accounted for using the time resistance concept (Janbu, 1985). This method has also been implemented in other constitutive models. In general two different strategies are used, isotaches of volumetric plastic strain, Vermeer and Neher (1999) or isotaches of the plastic multiplier, Grimstad and Degago (2010).

In addition, the time-dependent coupling between deformation and groundwater flow, as a result of excess pore water pressure generation, is accounted for by using a *consolidation* type analysis in PLAXIS.

An isotropic and Lode angle independent model was used in this study to simplify the model response.

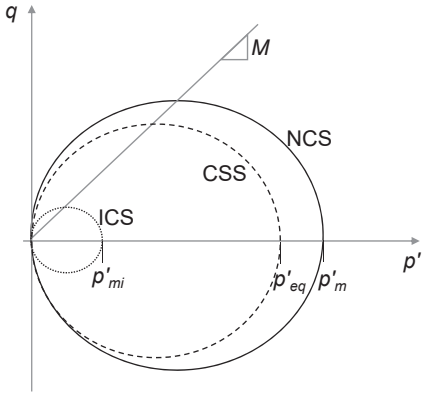

Fig. 2. Reference surfaces for the model: Current Stress Surface (CSS), Normal Consolidation Surface (NCS) and Intrinsic Compression Surface (ICS).

2.3. Model parameters

The soil parameters are based on low plasticity, highly sensitive clay from Tiller, Norway. The strain-softening and rate-dependent responses are displayed in Fig. 3 for an element test of an undrained isotropic triaxial compression test (CIUC). The peak undrained shear strength increases by 7 % for every tenfold increase in strain rate, and replicates the response of soft Scandinavian clays (Lunne and Andersen, 2007). The soil has a sensitivity, S_t, of 10, where sensitivity here is defined as $S_t = 1 + \chi$, and χ is the structure parameter.

Soil model parameters for the time-dependent model are provided in Table 1. The boundary value problem was initially tested with a non-softening material, these parameters are also provided.

The soil material had a unit weight of 10 kN/m^3 and the ground water level was at the ground surface (elevation zero), resulting in constant effective vertical stress with depth. A vertical preload of 100 kPa was applied to provide the initial stress condition. Constant effective stress was used to ensure constant mobilisation in the boundary value problem. The initial soil is slightly overconsolidated (compared to the 1-day reference) as the initial effective stress, p'_{eq} is 100 kPa and the effective preconsolidation pressure, p'_m is 105 kPa.

2.4. Numerical simulations

A bearing capacity boundary value problem was established with half the problem modelled, introducing symmetry: Fig. 4. The load was increased with different constant loading rates. The applied load was tapered off at the outer edge to avoid a singularity point. Loading rates were small enough to avoid inertia, thus quasi-static conditions prevailed. All analyses assumed small displacements and small strains.

Analyses were conducted in PLAXIS 2D v21, with the time dependent constitutive model implemented as a user-defined soil model. The bottom and left boundary were closed for pore water flow, but other boundaries remained open. The bottom boundary was fully fixed, left and right vertical boundaries were horizontally fixed, and the top soil boundary was fully free. Triangular 15-noded elements were used. Thus, the average nodal distance is a quarter of the element height.

Variations applied for the analyses:

1. Four different mesh discretisations were analysed to test for mesh dependency. The element size refers to the smallest element height in the area underneath the load where the shear band is expected to form. The element heights used were 0.009 m, 0.02 m, 0.05 m and 0.25 m. A larger element size of 0.5 m was initially tested, but was

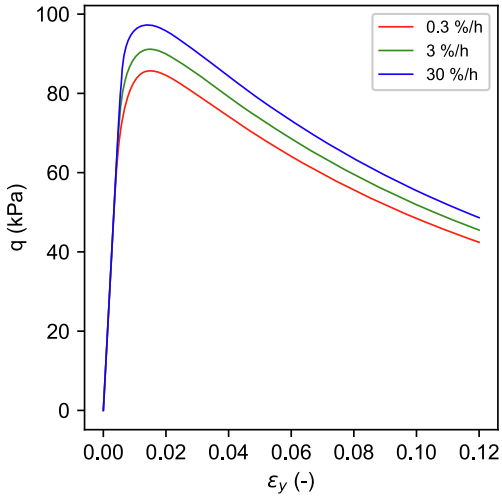

Fig. 3. Simulation of CIUC tests with three different strain rates, all three tests consolidated at 100 kPa confining pressure.

Table 1
Model parameters for the time-dependent model.

Parameter (Units)	Definition	Value Softening clay	Value Non-softening clay
K (kN/m^2)	Bulk modulus	5000	5000
G (kN/m^2)	Shear modulus	5000	5000
M (–)	Slope of critical state line in p'-q	1.5	1.5
ζ (–)	Irrecoverable compressibility, $\zeta = \lambda_i^* - \kappa^*$ [a]	0.048	0.048
χ_0 (–)	Initial value of structure	9	0
D (–)	Destructuration parameter	13	0
$p'_{mi,0}$ (kN/m^2)	Initial size of the intrinsic yield surface	10.5	105
β (–)	Creep ratio, $\beta = r_{si} \cdot \zeta$	32.5	32.5
$\dot{\lambda}_{ref}$(–)	Plastic multiplier at reference state, $\dot{\lambda}_{ref} = 1/(r_{si} \cdot \tau)$ [b,c]	1.5e-3	1.5e-3
$k_x = k_y$ (m/s)	Permeability	1e-9	1e-9

[a] λ_i^* is the modified compression index for a remoulded soil and κ^* is the modified swelling index.
[b] r_{si} is the creep number (Janbu, 1985) for a fully remoulded soil from an incremental loading oedometer test.
[c] τ is the reference time = 1 day (for 24 h incremental loading oedometer test).

found to be mesh-dependent for analyses without strain-softening material: the element size was too large.
2. The reference load (500 kPa) was applied using different loading rates to check if results remained mesh independent over different loading rates. The loading rates used were: 500 kPa/day, 50 MPa/day and 5 GPa/day.
3. Selected analyses were performed with permeability 100 times greater and a permeability of zero to study the effect of pore water flow. This set of analyses used 0.05 m elements and loading rate 500 kPa/day.

This paper investigates the shear band by studying the width of the softening zone, where softening soil is defined as the volume undergoing negative second order work, W_2^{int}:

$$W_2^{\text{int}} = {}^1\!/_2\, d\sigma^T d\varepsilon$$

For calculating the softening zone thickness, the stresses and strains were extracted for a section crossing the shear band perpendicularly at 1 m depth. PLAXIS interpolated the output values along these cross-sections, therefore the location of nodes around the cross-section had a small influence on the output values. Note that the focus of this paper was the size of the softening zone prior to and including failure.

Failure of a boundary value problem is defined as when deformations occur rapidly with little or no additional load. For this paper, the applied load is gradually increased until the system cannot support more, i.e. large deformations occur with little additional loading. A cut-off is applied when less than 1 kPa is required for a 1 m deformation directly beneath the centre of the load (coordinate (0, −1) in Fig. 4). The expected failure load is in the order of 270 kPa based on the Tresca criteria and a peak undrained shear strength of 45 kPa.

Strains were assessed using the deviatoric strain invariant, ε_q:

$$\varepsilon_q = \sqrt{\frac{2}{9}\left[(\varepsilon_{xx} - \varepsilon_{yy})^2 + (\varepsilon_{yy} - \varepsilon_{zz})^2 + (\varepsilon_{zz} - \varepsilon_{xx})^2\right] + \frac{1}{3}\left(\gamma_{xy}^2 + \gamma_{yz}^2 + \gamma_{zx}^2\right)}$$

3. Results

Failure occurred beneath the loaded area as a shear failure: Fig. 5. The strains localised at the same angle for all mesh sizes and loading rates. The total strains at failure were alike for the 0.009 m, 0.02 m and 0.05 m element sizes, but the 0.25 m mesh size had a wider localised zone and was mesh dependent.

Load-displacement curves (Fig. 6) demonstrate that results for the different mesh discretisations were almost identical, only the coarsest mesh (0.25 m) displayed a different response at failure. The details at failure are presented in Fig. 7: all plots stop at the same gradient (1 kPa/m displacement), but the transfer to the failure mechanism occurs rapidly for the 0.009 m element size and is not visible at this scale. The transition to failure is achieved with a smooth, continuous line for all cases.

The applied soil model provided a mesh independent failure load for each loading rate. The failure loads for all mesh sizes and loading times are presented in Table 2. As expected, the failure loads were higher for the faster rates, and the loading rate 500 kPa/day (similar loading rate

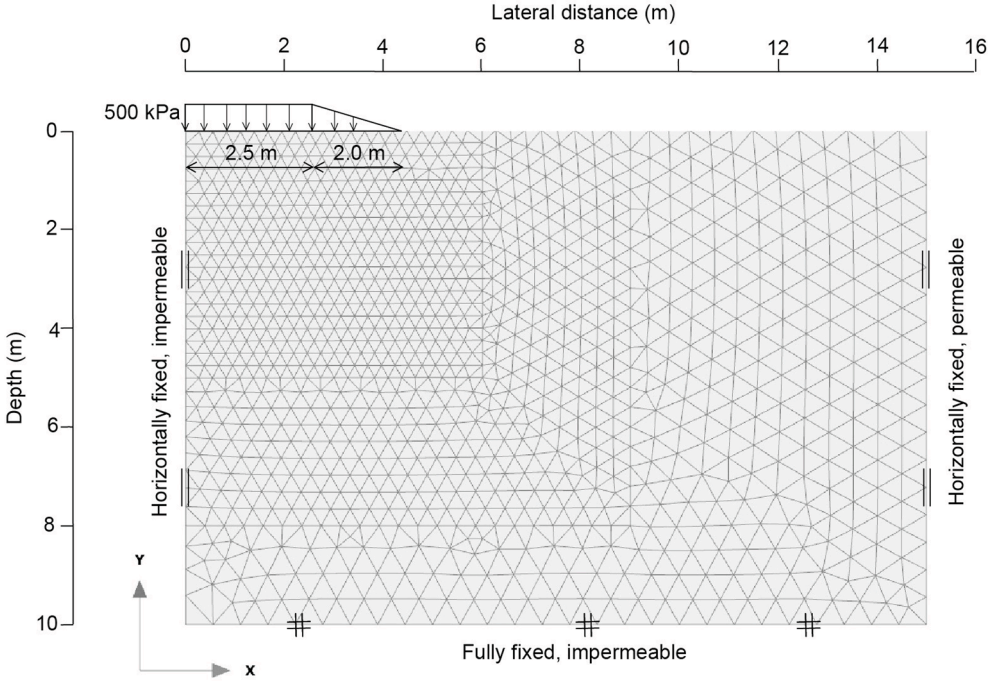

Fig. 4. Bearing capacity problem (displaying the coarsest discretisation with element size = 0.25 m beneath load).

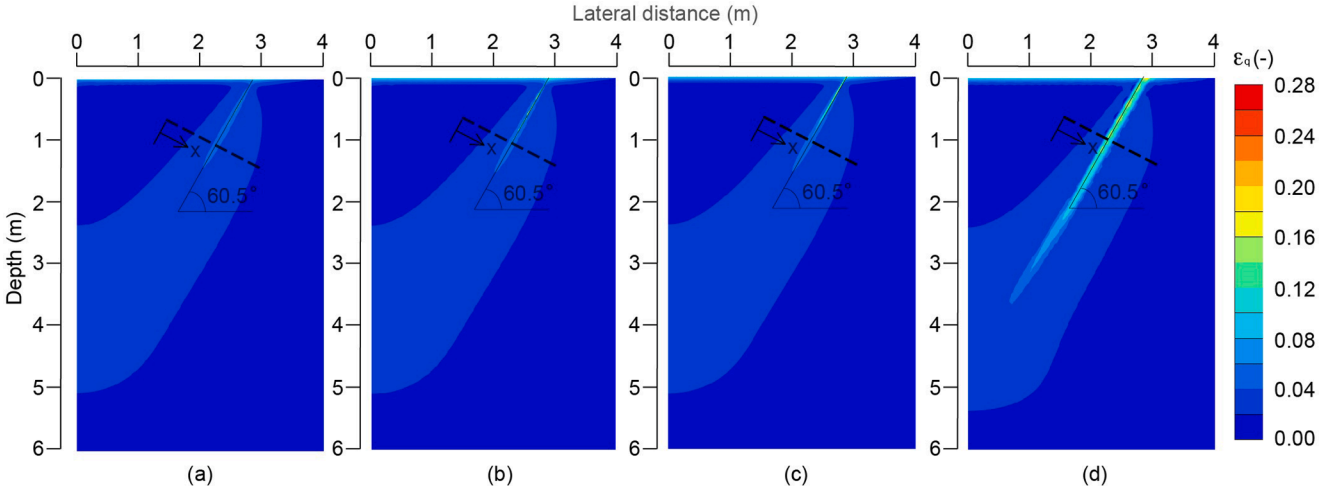

Fig. 5. Total deviatoric strain distribution underneath the loading area at the state of failure (peak load) for different element sizes: a) 0.009 m, b) 0.02 m, c) 0.05 m and d) 0.25 m. Loading rate = 500 kPa/day. Location of cross-section depicted by dashed line.

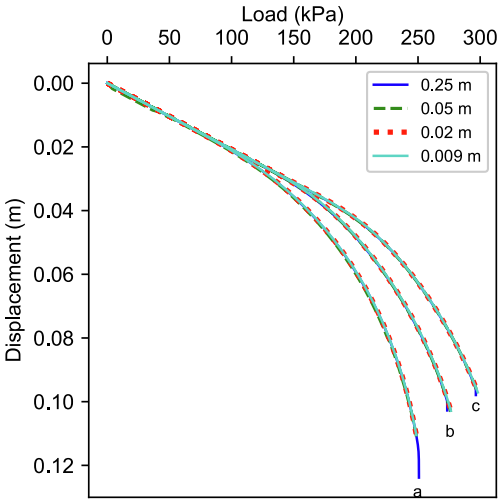

Fig. 6. Vertical displacement beneath load for different element sizes and loading rates: a) 500 kPa/day, b) 50 MPa/day and c) 5 GPa/day. The detail at failure is presented in Fig. 7.

to those used in incremental loading oedometer test) gives a failure load around that predicted by the Tresca criterion (270 kPa).

The strain and strain rate distributions for a cross-section through the softening zone (Fig. 8: left and middle column) show that the 0.009 m, 0.02 m and 0.05 m element sizes had identical results until just prior to failure. The results for 0.25 m element size gradually diverge from the 0.009 m, 0.02 m and 0.05 m results, indicating a slight mesh dependency for the larger element size, however it does not affect the failure load significantly. The deviatoric stress (q) within the softening zone decreases as the load increases.

Whilst the strains increasingly concentrate in the centre of the softening zone (Fig. 8), the thicknesses of the softening zones increase whilst remaining very similar for all element sizes, presented for the loading rate 500 kPa/day in Fig. 9. The softening commenced at the same applied load (223 kPa) for all element sizes and the softening zone grew

Table 2
Failure loads for different element sizes and different loading rates.

Loading rate	Element size (m)	Failure load (kPa)
5 GPa/day	0.009	298.1
	0.02	297.5
	0.05	296.8
	0.25	296.5
50 MPa/day	0.009	276.4
	0.02	276.5
	0.05	276.5
	0.25	273.5
500 kPa/day	0.009	248.6
	0.02	248.7
	0.05	248.7
	0.25	250.7

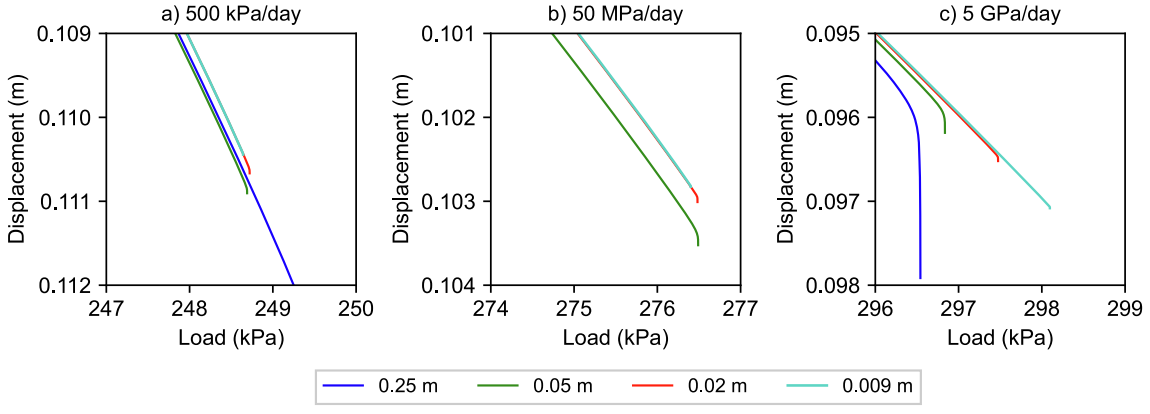

Fig. 7. Detail at failure for the load–displacement plots from Fig. 6, with analyses using different element sizes and loading rates.

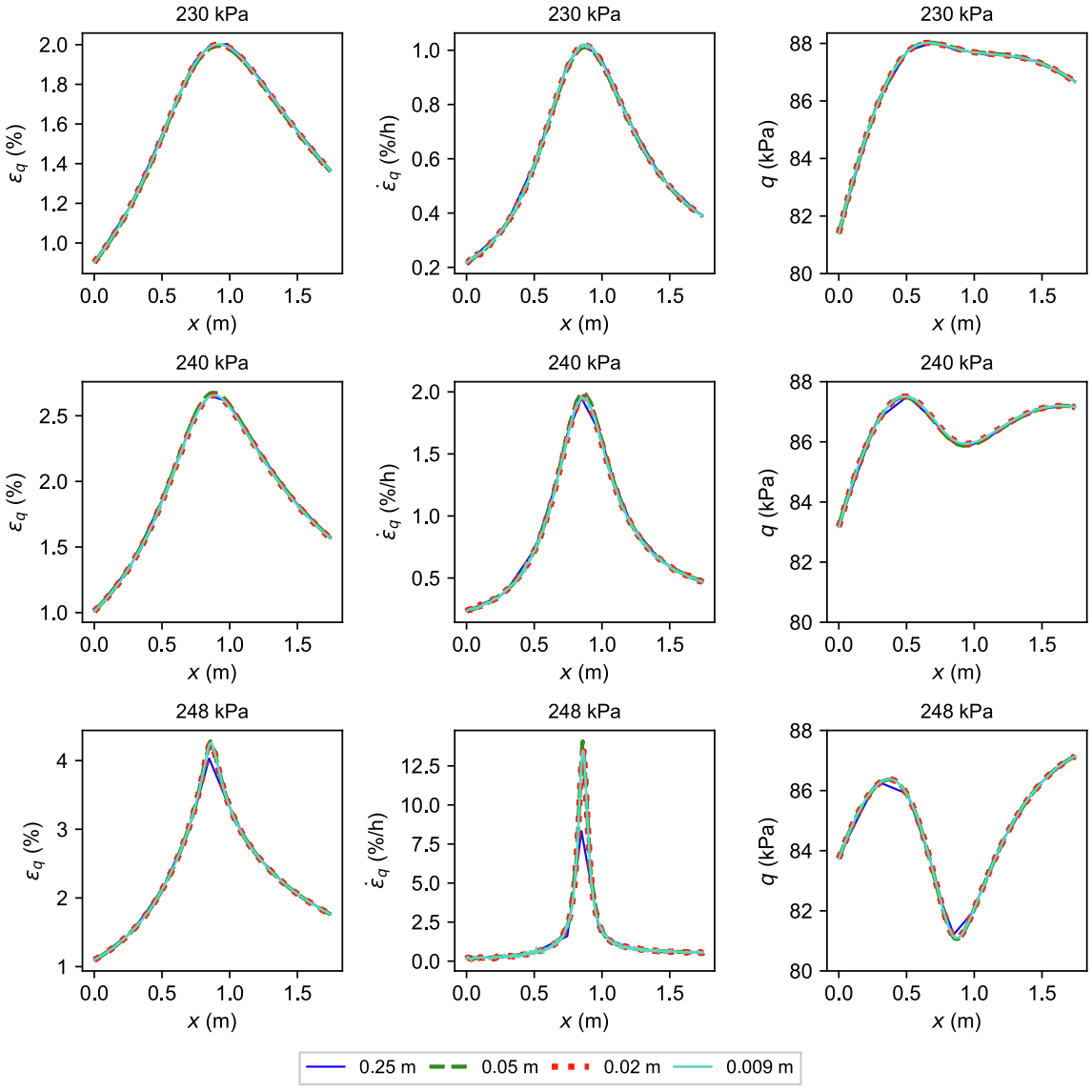

Fig. 8. Distribution of deviatoric strain (ε_q), strain rate ($\dot{\varepsilon}_q$) and deviatoric stress invariant (q) for a cross-section at 1 m depth using four different mesh discretisations. Results are depicted at three load stages: applied load = 230 kPa, 240 kPa and 248 kPa. Loading rate = 500 kPa/day.

in width until reaching 99 % of the failure load. Whilst the total width of the softening area widens up to 1.4 m, the negative work increasingly concentrates in the centre of the shear band: Fig. 10.

Just prior to failure, between 248.5 kPa and 248.6 kPa in Fig. 10, the second order work becomes positive: this may be due to numerical instabilities as the concentrated strains in the centre of the softening zone attempt to become narrower than the mesh discretisation allows. The plots displaying softening zone thickness (Figs. 9 and 14) were thus terminated when the centre of the softening zone started to harden.

The maximum thickness of the softening zone was smaller for faster loading rates: Fig. 11. The difference is attributed to the generation and dissipation of excess pore water pressure, as viscoplasticity alone would result in the same shear strength changes and thus the same shear band thickness. The failure load was similarly affected by pore water flow: the percentage difference in failure load per hundredfold change in loading rate were not equal (11.2 % and 7.6 % for the 0.02 m element size), with a larger difference at slower rates when there is more time for pore water flow to occur.

Depending on the distance of the stress point from the centre of the softening zone, the stress paths differed (Fig. 12): due to local variations in both strain rate and pore water flow. The material on the edge and

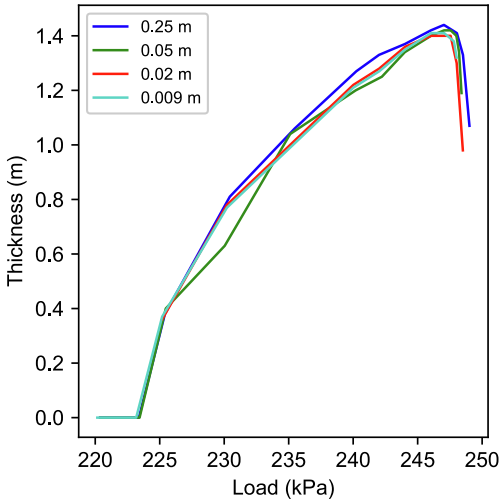

Fig. 9. Thickness of softening zone at 1 m depth for different mesh discretisations. For analyses with loading rate = 500 kPa/day.

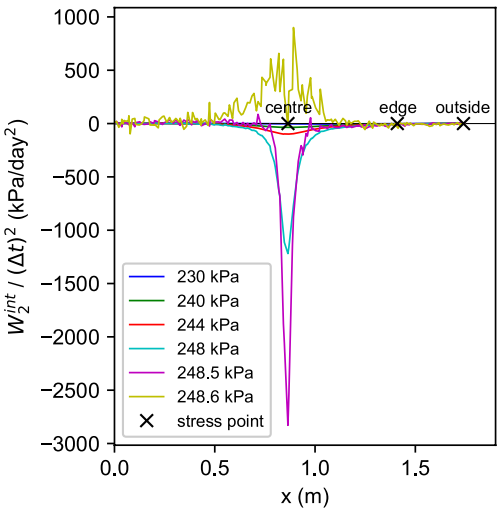

Fig. 10. Distribution of second order work at various loading stages. Location of selected stress points also shown. Work is normalised by time step, $(\Delta t)^2$, because the step size reduces during the analysis. For element size = 0.02 m and loading rate = 500 kPa/day.

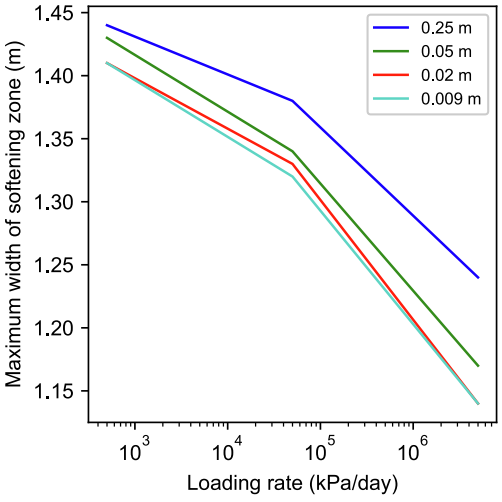

Fig. 11. Maximum thickness of softening zone at 1 m depth for different element sizes and loading rates.

outside the softening zone experienced higher effective stresses and were further from critical state. Isolating the effect of pore water flow on this set of results was not possible, therefore the effect of increased pore water flow was studied further by varying the permeability (k).

As the analyses approached failure, the centre of the softening zone abruptly started hardening (Fig. 12), again, this reflects the start of numerical instability at failure. The problem is attributed to the large strain gradient over the centre elements and inability of the finite element formulation to maintain stress equilibrium. Numerical issues may also arise at failure due to the bearing capacity problem being load controlled; issues occur as the total resistance of the soil becomes lower than the applied load.

Changing the permeability to zero resulted in only a slight decrease in failure load (Table 3), indicating that the base case is almost fully undrained. Increasing the permeability led to higher failure loads. Changing the permeability also resulted in changes in pore pressures, stress paths, strains and strain rates: results are presented in Fig. 13.

For zero permeability, the results were extremely close to the base case ($k = 10^{-9}$ m/s); however, it is apparent that allowing pore water flow enabled the material in the centre of the shear band to strain to

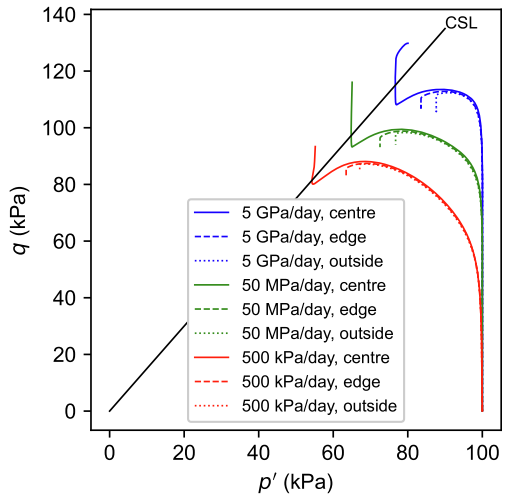

Fig. 12. Stress paths for material at various distances from centre of softening zone. Stress points are located along the cross-section as indicated in Fig. 10. For element size = 0.05 m and loading rate = 500 kPa/day.

Table 3
Failure loads for different element sizes and different permeabilities.

Permeability (m/s)	Failure load (kPa)	Difference to base case (%)
0	246.6	−0.9
10^{-9} (base case)	248.7	0
10^{-7}	270.3	8.7

larger strains. The growth of the softening zone (Fig. 14) for zero permeability was also similar to the base case, but the softening zone does not reduce in thickness prior to failure: the centre of the zone began to harden whilst the outer edges were still strain-softening.

When the permeability was increased hundredfold, the following were noted:

- The initial response was partially drained (Fig. 13b) before the strain rate increased (Fig. 13c) and response became more similar to undrained.
- Increased drainage inhibited strain-softening. The centre of the softening zone barely strain-softened, whilst outside the softening zone the material only hardened prior to unloading (Fig. 13a).
- The strain rates were initially higher than those of the base case (up to load 230 kPa), however high strain rates could be maintained for longer. Strain acceleration and thus failure occurred at a larger load.
- The changes in excess pore pressure, Δu, were lower at all stress points (Fig. 13d), contributing to higher effective stresses. Lower pore pressures were a result of i) higher strain rates, and ii) higher permeability and flow of pore water.
- Later development of strain-softening and a thinner softening zone: Fig. 14.

4. Discussion

The objective of this paper is to investigate if a strain-rate dependent soil model used in combination with coupled pore water flow generates mesh independent results for a bearing capacity problem in a soft strain-softening clay. Results show that the failure load and the soil displacements were the same for different mesh discretisations. As for any finite element modelling study, the inherent discretisation errors required a study of mesh size. In this particular problem, an element size of 1/20 of the foundation size was sufficiently small to define the failure loads whilst using 15-noded triangular elements.

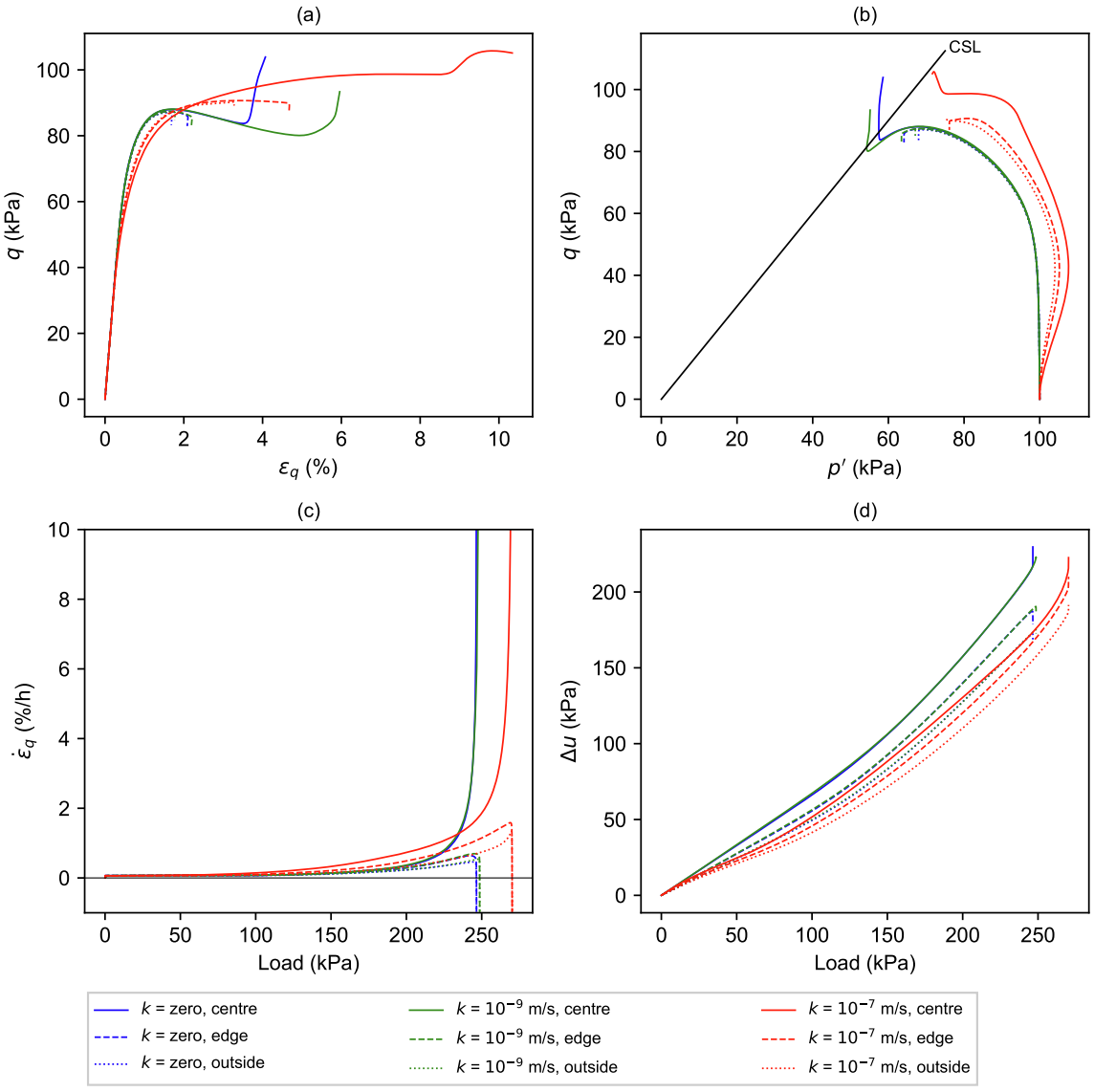

Fig. 13. Material response for analyses with different permeabilities. Stress points are located along the cross-section as indicated in Fig. 10. For element size = 0.05 m and loading rate = 500 kPa/day.

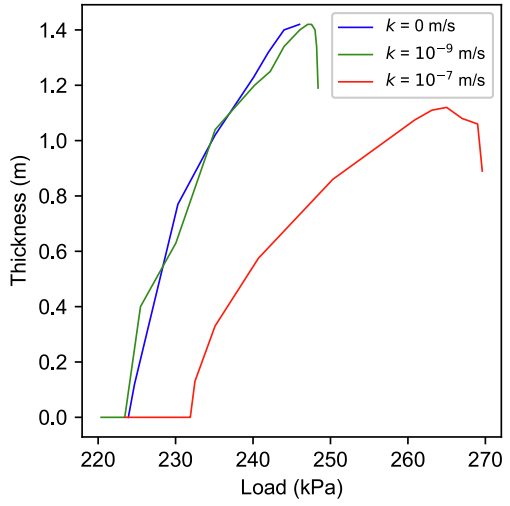

Fig. 14. Thickness of softening zone at 1 m depth for different permeabilities. For element size = 0.05 m and loading rate = 500 kPa/day.

4.1. Regularisation ability of rate-dependency and pore water flow

The regularising effect of this rate dependent formulation was demonstrated by a one-dimensional problem in Rødvand et al. (2022). The rate-dependent constitutive model allows equal shear stresses to be achieved by straining at different rates, but at different strain and effective stress levels: Fig. 13. Similar to the one-dimensional problem, the results from the bearing capacity problem are only regularised up to a certain point, but the period of mesh independent results is sufficient to calculate a failure load that is unaffected by mesh discretisation. The post failure response cannot be analysed for this boundary value problem as the analyses are load controlled.

In the soft, contractive marine clay studied here, dissipation of shear induced excess pore pressure out of the softening zone slightly assists the regularisation process by increasing the effective stress and shear strength in the softening zone. The undrained analysis (given as $k = 0$) had slightly lower failure load than the analysis with $k = 10^{-9}$ m/s, but experienced similar responses prior to failure, thus indicating that for large scale problems undergoing rapid loading, the flow of pore water at the moment of failure does not play a large role in the failure mechanism. Increasing the permeability a hundredfold to $k = 10^{-7}$ m/s almost

prevented the occurrence of strain-softening and resulted in an increased failure load. Therefore, it is also expected that for smaller problems, with shorter drainage paths (e.g. penetration of CPT cone or t-bar), the effect of permeability and pore water flow will have a larger effect on strain localisation and the failure load.

4.2. Softening zone and shear zone

Rather than use the term the "shear band" in the results section, the authors found it more correct to adopt the term the *softening zone*. The definition of a shear band varies in literature. In rate independent elastoplastic analyses, the shear band is bounded by the unloading soil outside the shear band. In dynamic (dispersion) analyses, a limit may be applied to the relative strain rates, e.g. Wang et al. (1996) used 1 % of the maximum strain rate to define the outer edge of the shear band. If these definitions of shear band are used, then the bearing capacity problem reaches failure before a shear band forms.

The width of the softening zone is in the order of meters (up to 1.45 m wide) and is therefore akin to Leroueil's (2001) definition of a *weakened zone*, rather than the typical width of a shear band i.e. millimetre to centimetre scale. Whilst this weakened zone has been observed in the field, it is not normally assessed using strain-softening models in numerical analyses. The width of the softening zone governs the failure load for the bearing capacity problem studied. The thinning of the softening zone and continued localisation of strains at failure may correspond to the formation of the *shear zone* or *slip surface*.

The formation of a shear zone requires the reorientation of clay particles and leads to deformation patterns (Riedel shears and thrust shears) that are visible at microscopic scale (Skempton, 1966; Ahlgren, 2001). Gylland et al. (2014) observed that the shear zone only developed in the post peak range of modified triaxial experiments however a smooth localised zone was visible prior to failure; this smooth localised zone may correspond to the softening zone found in this research paper. Gylland's findings corroborate the numerical results: that the softening zone thickness governs the determination of the failure load, whilst the thinner shear zone is relevant for the post-failure and large strain response.

This study indicates that we do not need to study the strain localisation of clay materials at particle scale. Rather, the weakened zone created by strain-softening is critical for determination of failure loads for strain-softening clays. This is positive news for large boundary value problems: analyses can continue to be conducted using continuum mechanics and finite element analyses, avoiding the need to conduct analyses at particle scale. The size of the weakened zone will depend on many factors, also some that are outside the remits of the current study, such as pore pressure gradient and dimensions of problem (Thakur, 2011). Thus, it is expected that the width of the softening zone, and consequently the failure load, will also differ somewhat as these parameters are varied: a further study of these factors would be useful.

The bearing capacity problem studied gave insight into the regularisation ability of the constitutive model and also the growth of the shear band in the lead up to failure. The strain localisation process will be similar for other boundary value problems with sensitive clays, such as excavations or slope stability problems triggered by significant stress changes due to either erosion at the toe of the slope or loading at the slope crest. It is not expected that analyses of further boundary value problems will provide additional insight into the regularisation mechanism.

Other strain-rate models for structured clay that have been published but not tested for mesh dependency using failure problems (no strain localisation occurs) include Grimstad and Degago (2010), Yin and Karstunen (2011), Rezania et al. (2016) and Gras et al. (2018). These models potentially have the same regularising capability as the model tested in this paper.

5. Conclusions

Using realistic rate dependency and permeability parameters, the regularising ability of a rate dependent material model coupled with pore water flow was investigated for a bearing capacity failure in a soft strain-softening clay. Analyses using the constitutive model were shown to calculate mesh independent failure loads for a large range of loading rates, whilst using a parameters representative of a sensitive Scandinavian clay. Rate dependency was the key regularisation process, whilst pore water flow was shown to only slightly delay failure in clay with low permeability.

Prior to failure, strains localised in a softening zone where material underwent strain-softening. The width of this softening zone was mesh-independent. The maximum width of the softening zone grew to over 1 m, even whilst the strains became increasingly concentrated in the centre of the softening zone. Numerical issues were encountered at failure but did not appear to significantly affect the failure load for the different mesh sizes when sufficiently small element sizes were used. Thus, the rate dependent model was satisfactory at generating mesh independent failure loads and it demonstrates that it is not necessary to analyse failure problems in strain-softening clays at particle scale.

Funding

The main author gratefully acknowledges the STIPINST funding (nr. 259863) from the Research Council of Norway (RCN) and funding from the Norwegian Geotechnical Institute (NGI).

CRediT authorship contribution statement

Laura Rødvand: Conceptualization, Methodology, Formal analysis, Writing – original draft. **Hans Petter Jostad:** Supervision, Writing – review & editing. **Gustav Grimstad:** Software, Writing – review & editing. **Lars Andresen:** Writing – review & editing.

Declaration of Competing Interest

The authors declare that they have no known competing financial interests or personal relationships that could have appeared to influence the work reported in this paper.

Data availability

Data will be made available on request.

Acknowledgements

We thank Jon Rønningen for his assistance in implementing the constitutive model.

References

Ahlgren, S., 2001. The nucleation and evolution of Riedel shear zones as deformation bands in porous sandstone. J. Struct. Geol. 23 (8), 1203–1214. https://doi.org/10.1016/S0191-8141(00)00183-8.

Bazant, Z.P., Belytschko, T.B., Chang, T., 1984. Continuum theory for strain-softening. 110(12), pp. 1666–1692.

Conte, E., Silvestri, F., Troncone, A., 2010. Stability analysis of slopes in soils with strain-softening behaviour. Comput. Geotech. 37 (5), 710–722. https://doi.org/10.1016/j.compgeo.2010.04.010.

de Borst, R., Duretz, T., 2020. On viscoplastic regularisation of strain-softening rocks and soils. Int. J. Numer. Anal. Meth. Geomech. 44 (6), 890–903. https://doi.org/10.1002/nag.3046.

di Prisco, C., Imposimato, S., Aifantis, E.C., 2002. A visco-plastic constitutive model for granular soils modified according to non-local and gradient approaches. Int. J. Numer. Anal. Meth. Geomech. 26, 121–138. https://doi.org/10.1002/nag.195.

Eringen, A.C., 1981. On nonlocal plasticity. Int. J. Eng. Sci. 19 (12), 1461–1474. https://doi.org/10.1016/0020-7225(81)90072-0.

Gens, A., Nova, R., 1993. Conceptual bases for a constitutive model for bonded soils and weak rocks. In: Geotechnical Engineering of Hard Soils – Soft Rocks. Rotterdam, pp. 485–494.

Gras, J.P., et al., 2018. Permissible range of model parameters for natural fine-grained materials. Acta Geotech. 13 (2), 387–398. https://doi.org/10.1007/s11440-017-0553-1.

Grimstad, G., Degago, S., 2010. A non-associated creep model for structured anisotropic clay (n-SAC). In: Numerical Methods in Geotechnical Engineering. CRC Press, pp. 3–8. https://doi.org/10.1201/b10551-3.

Gylland, A.S., Jostad, H.P., Nordal, S., 2014. Experimental study of strain localization in sensitive clays. Acta Geotech. 9 (2), 227–240. https://doi.org/10.1007/s11440-013-0217-8.

Janbu, N., 1985. Soil models in offshore engineering. Géotechnique 35 (3), 241–281. https://doi.org/10.1680/geot.1985.35.3.241.

Jostad, H.P., Andresen, L., Thakur, V., 2006. Calculation of shear band thickness in sensitive clays. In: Numerical Methods in Geotechnical Engineering. Taylor & Francis, pp. 27–32. doi: 10.1201/9781439833766.ch4.

Leroueil, S., 2001. Natural slopes and cuts: movement and failure mechanisms. Géotechnique 51 (3), 197–243. https://doi.org/10.1680/geot.2001.51.3.197.

Loret, B., Prevost, J.H., 1991. Dynamic Strain Localization in Fluid-Saturated Porous Media. J. Eng. Mech. 117 (4), 907–922. https://doi.org/10.1061/(ASCE)0733-9399(1991)117:4(907).

Lunne, T., Andersen, K.H., 2007. Soft clay shear strength parameters for deepwater geotechnical design. In: Proceedings of the 6th International Off shore Site Investigation and Geotechnics Conference. London.

Oka, F., Adachi, T., Yashima, A., 1995. A strain localization analysis using a viscoplastic softening model for clay. Int. J. Plast 11 (5), 523–545.

Oka, F., et al., 2005. Strain localization of rectangular clay specimen under undrained triaxial compression conditions. In: Proceedings of the 16th International Conference on Soil Mechanics and Geotechnical Engineering: Geotechnology in Harmony with the Global Environment, 2, pp. 841–844. doi: 10.3233/978-1-61499-656-9-841.

Potts, D.M., Dounias, G.T., Vaughan, P.R., 1990. Finite element analysis of progressive failure of Carsington embankment. Géotechnique 40 (1), 79–101. https://doi.org/10.1680/geot.1990.40.1.79.

Rezania, M., Taiebat, M., Poletti, E., 2016. A viscoplastic SANICLAY model for natural soft soils. Comput. Geotech. 73, 128–141. https://doi.org/10.1016/j.compgeo.2015.11.023.

Rødvand, L.A., et al., 2022. Strain localisation in sensitive clays: can rate dependency provide mesh independent results? Comput. Geotech. 145, 104678 https://doi.org/10.1016/j.compgeo.2022.104678.

Skempton, A.W., 1966. Some observations on tectonic shear zones. In: 1st Int. Soc. Rock Mech. Congr. Lisbon, pp. 329–335.

Sluys, L.J., de Borst, R., 1992. Wave propagation and localization in a rate-dependent cracked medium—model formulation and one-dimensional examples. Int. J. Solids Struct. 29 (23), 2945–2958. https://doi.org/10.1016/0020-7683(92)90151-I.

Thakur, V., 2011. Numerically observed shear bands in soft sensitive clays. Geomech. Geoeng. 6 (2), 131–146. https://doi.org/10.1080/17486025.2010.546434.

Thakur, V., et al., 2018. Shear bands in undrained plane strain compression of Norwegian quick clays. Can. Geotech. J. 55 (1), 45–56. https://doi.org/10.1139/cgj-2016-0443.

Thakur, V., et al., 2014. 'How Well Do We Understand the Undrained Strain Softening Response in Soft Sensitive Clays?. In: Advances in Natural and Technological Hazards Research, pp. 291–303. doi: 10.1007/978-94-007-7079-9_23.

Vermeer, P.A., Neher, H.P., 1999. A soft soil model that accounts for creep. In: Brinkgreve, R.B. (Ed.), Beyond 2000 in Computational Geotechnics. Rotterdam, pp. 249–261. doi: 10.1201/9781315138206-24.

Viggiani, G., Küntz, M., Desrues, J., 2001. An experimental investigation of the relationships between grain size distribution and shear banding in sand. In: Vermeer, P.A. (Ed.), Continuous and Discontinuous Modelling of Cohesive-Frictional Materials. Springer, Berlin Heidelberg, pp. 111–127. https://doi.org/10.1007/3-540-44424-6_8.

Wang, W.M., Sluys, L.J., De Borst, R., 1996. Interaction between material length scale and imperfection size for localisation phenomena in viscoplastic media. Eur. J. Mech., A/Solids 15 (3), 447–464.

Yin, Z.-Y., Karstunen, M., 2011. Modelling strain-rate-dependency of natural soft clays combined with anisotropy and destructuration. Acta Mech. Solida Sin. 24 (3), 216–230. https://doi.org/10.1016/S0894-9166(11)60023-2.